

Dynamics of graphene growth on a metal surface: a time-dependent photoemission study

Alexander Grüneis^{1,2}, Kurt Kummer³ and Denis V. Vyalikh³

¹*Faculty of Physics, University of Vienna,
Boltzmannngasse 5, A-1090 Vienna, Austria*

²*IFW–Dresden, P.O. Box 270116, D-01171 Dresden, Germany and*

³*Institute of Solid State Physics, Dresden University
of Technology, D-01062 Dresden, Germany*

Abstract

Applying time-dependent photoemission we unravel the graphene growth process on a metallic surface by chemical vapor deposition (CVD). Graphene CVD growth is in stark contrast to the standard growth process of two-dimensional films because it is self-limiting and stops as soon as a monolayer graphene has been synthesized. Most importantly, a novel phase of metastable graphene was discovered that is characterized by permanent and simultaneous construction and deconstruction. The high quality and large area graphene flakes are characterized by angle-resolved photoemission proofing that they are indeed monolayer and cover the whole 1×1 cm Nickel substrate. These findings are of high relevance to the intensive search for reliable synthesis methods for large graphene flakes of controlled layer number.

Its astonishing electronic properties have placed graphene, a planar sheet of carbon atoms packed in honeycomb structure, in the focus of considerable current research efforts.[1, 2] The occurrence of Dirac Fermions at low energies and the remarkably high electron mobility have raised high expectations regarding its future use as an active element in nanoelectronics and hybrid materials. Moreover, graphene is highly promising to play a crucial role in future spintronic applications and can serve as an effective oxidation protection when grown epitaxially on metal surfaces.[3]

Naturally these findings have stimulated the development of efficient and reliable synthesis protocols for high-quality graphene layers. To date several techniques were established: (i) precipitation from silicon carbide [4], (ii) mechanical exfoliation from graphite [5], (iii) reduction of exfoliated graphite oxide [6, 7, 8], (iv) thermal expansion of graphite oxide [9], (v) laser desorption [10], and (vi) growth by chemical vapor deposition (CVD) on metal surfaces [11, 12, 13]. The latter is especially interesting for ferromagnetic materials and it was demonstrated that spin polarization of a Ni(111) substrate can be cloned almost completely into a graphene overlayer [14]. This allows to design sources of spin polarized electrons which are fully prevented from aging when exposed to reactive gases. Despite these promising perspectives, little is known about the actual growth mechanism of graphene on metal surfaces [15].

Here we show that the high spatial compatibility of the Ni(111) surface and the graphene sheet makes it a perfect system to study functional synthesis of monolayer graphene on metal substrates by a self limiting CVD process. The high crystallinity and large area growth of monolayer graphene is unambiguously proven by angle-resolved photoemission spectroscopy (ARPES) of the electronic band structure. For CVD of the graphene layer, a freshly prepared Ni(111) substrate was heated and stabilized at the desired synthesis temperature first. Then propylene gas (C_3H_6), which served as the carbon source, was introduced into the chamber. Doing so the gas pressure was adjusted to 2×10^{-7} mbar using a leak valve. In the incipient reaction of propylene with the Ni surface a graphene monolayer is formed as evidenced by the appearance of a single π band by ARPES as will be shown later. During the whole synthesis procedure the C 1s signal was recorded together with the C_3H_6 gas pressure and the substrate temperature. This complete set of information allowed us to monitor the full growth process dependent on time. One time-dependent data set during the graphene CVD is shown in 1. Starting from a blank Ni film kept at room temperature it shows the

time evolution of (a) the raw PE signal in the C 1s range, (b) the C₃H₆ partial pressure, (c) and (d) the C 1s signal intensity integrated for a range of ± 0.5 eV around the blue and green lines in (a), respectively. Considering the C 1s spectra it is evident that in the beginning the prepared Ni(111) surface still shows small signs of carboneous contaminations at 283 eV binding energy (BE). They however are fully removed during the first 200 s when the substrate temperature is raised to the synthesis temperature for the graphene growth. After the substrate is stabilized in temperature the leak valve to the C₃H₆ gas inlet is opened (this point corresponds to a time $t \sim 500$ s). Immediately with increasing C₃H₆ pressure a distinct peak at 283 eV BE arises. Only at $t \sim 600$ s the graphene related peak at 284.7 eV starts to grow (see the dashed lines in 1b–d).

Three origins of the 283 eV peak are conceivable: (i) unfragmented C₃H₆, (ii) surface nickel carbide and (iii) C₃H₆ fragments. The former two, however, are not supported by additionally performed experiments. First, producing a C₃H₆ film on Ni(111) by room temperature adsorption we found the C 1s PE peak at ~ 284 eV BE and not at 283 eV BE (not shown). Secondly, we have deliberately synthesized nickel carbide and proofed this by LEED as described previously [16]. We indeed detected the C 1s peak at 283 eV BE, in agreement with literature values [17] for nickel carbide. But we were not able to convert the surface nickel carbide film into graphene by heating. Instead we observed that the nickel carbide film is stable and the peak at 283 eV did not vanish nor did appear a graphene peak. Thus we conclude that the observed peak at 283 eV BE is due to C₃H₆ fragments and in agreement to previous literatures that report a very similar experiment of carbon monoxide decomposition on Rh, we assign it partly to atomic carbon [18]. Another contribution to this peak might be edge atoms of the growing graphene film. Indeed, this would explain why the intensity decreases as the graphene layer forms and has fewer edge atoms. Our assignment is also consistent with the fact that we did not observe any sign of C-H bonds, which appear as a sideband in the C 1s peak at ~ 1 eV higher binding energy than the graphene peak [19].

Looking at 1c and d one recognizes that during construction of the graphene network a major part of the fragments vanish, i.e. are transformed into graphene. When the graphene growth is completed only a minor fraction of fragments remains. For all recorded spectra the beginning of both the graphene peak rise and the fragment peak decline coincide in time. Comparing the maximum intensity of the fragment peak (~ 0.7 a.u., 1c) and graphene peak (~ 2.5 a.u., 1d) it becomes apparent that there must be an additional major path of carbon

incorporation to achieve a complete monolayer. We believe that graphene nucleates initially from fragments that sit on edges and defects of the Ni surface. The part missing to a full graphene monolayer grows by attachment of carbons.

The percentage of fragments in the final graphene layer depends considerably on the synthesis temperature as shown in 2a. While clearly present for lower synthesis temperatures a distinct fragment peak is not observed beyond $\sim 600^\circ\text{C}$. This highlights that high temperatures result in an efficient conversion of fragments to graphene. The quantitative comparison of the fragment PE and the graphene PE intensities in 2b reveals a decline in their ratio from 10% to about 1% when going from 345°C to 669°C . The high structural quality of the graphene layer synthesized at 669°C is confirmed by least-squares fit analysis of the C 1s PE spectrum. Using a single component with Doniach-Sunjc lineshape we obtained $\Gamma_l=216$ meV and $\alpha = 0.1$ for the intrinsic line width and asymmetry parameter, respectively which is in agreement to previously reported values.[20]

The synthesis temperature is decisive not only for the structural quality of the graphene layer, it furthermore governs the graphene growth rate. In 3(a) the time evolution of the graphene PE intensity is shown for increasing temperatures. For the purpose of comparison the curves were aligned to each another on the time scale. Taking the slope of the C 1s intensity of graphene at the turning point of the curve as a measure for the growth rate we found that the latter has a synthesis temperature dependence as shown in 3b. For temperatures below 350°C no extensive graphene growth occurs. Then a rapid increase in the growth rate is observed when the synthesis temperature is raised to about 500°C . Beginning from 500°C the growth rate remains constant before it appears to decline again above 650°C . In contrast to graphene layers synthesized at lower temperatures, we found that those constructed at 657°C and 669°C exist only in a metastable phase.

In 3c we show a full data set of propylene pressure and fragment and graphene C 1s PE intensities for $T=669^\circ\text{C}$. When propylene is introduced into the chamber the graphene grows up to completion of one monolayer. However, after a closed graphene layer is reached and the gas inlet closed, the graphene C 1s intensity decreases, unless the temperature has been lowered before. The graphene layer completely disappears in 400s after the carbon supply has been turned off.

Two possible reasons for the disappearance of graphene carbon atoms are conceivable. First, it may be possible that at such high temperatures carbon atoms in graphene react with

residual gases in the chamber, e.g. hydrogen, and form hydrocarbons which can easily desorb. Secondly, diffusion of carbon atoms into the bulk Ni could set in for the highest applied temperatures [21, 22, 23]. The question, whether desorption or diffusion is dominating remains subject to further investigations. We wish to point out that after high-temperature deconstruction of the graphene layer no notable amount of carbon remains on the surface. In fact, after repeated synthesis and heating procedures we always found a pristine Ni surface, ready for a new cycle of graphene growth.

Finally, we demonstrate the high crystallinity of a graphene monolayer synthesized at 550°C by performing a mapping of the electronic band structure using ARPES. The measured band structure between Γ and K points in the two-dimensional Brillouin zone is shown in 4a. The appearance of π and σ bands is a clear indication for long range crystallinity and few defects in the honeycomb lattice. Furthermore a gap at K point appears which is a result of substrate interaction and hybridization of C $2p_z$ and Ni $3d_{3z^2-r^2}$ orbitals as discussed previously [11]. In 4b the corresponding raw spectra are depicted. It can be seen from the ARPES results that only one π valence band is visible. This demonstrates unambiguously that we have indeed synthesized monolayer graphene as a graphene bilayer would have two π bands. The ARPES spectra are also strongly supporting the observation from the time-resolved photoemission that the catalytic activity diminishes after the growth of one monolayer.

In summary, applying time-resolved PES we were able to observe and characterize the dependence of graphene quality and growth rate on the synthesis temperature, for the first time. For high temperatures above 650°C we found the graphene layer in a metastable state characterized by permanent simultaneous construction and deconstruction. The high crystallinity of the synthesized graphene monolayers was confirmed by a mapping of the electronic band structure by ARPES.

Experimental

The Ni films were grown onto a W(110) single crystal which could be heated from the backside by electron bombardment. The temperature was monitored using a thermocouple which was spot welded on the back side of the tungsten crystal to ensure good thermal contact. During deposition the tungsten crystal was heated to constant 150°C from the backside

by electron beam. The W(110) surface was cleaned by repeated cycles of short flashes up to 1700°C and annealing in oxygen at 1000°C. Subsequently, a Ni film of 10 nm thickness was deposited on the W(110) surface by electron beam evaporation from a Ni rod (99.9% purity). The Ni film thickness was monitored by a quartz microbalance. Nickel grows epitaxially in (111) fashion on W(110) [24] and we further employ it as a catalytic template for graphene CVD due to its small lattice mismatch. Low energy electron diffraction (LEED) and photoelectron spectroscopy (PES) were utilized to check the W(110) and Ni(111) surfaces for order and cleanliness [11, 24]. For all experiments the base pressure before dosing C₃H₆ was better than 5×10^{-10} mbar, during Ni evaporation better than 2×10^{-9} mbar. Time-dependent experiments were carried out at the SuperESCA beamline of the ELETTRA synchrotron (Trieste, Italy). The C 1s spectra were recorded at $h\nu=400$ eV photon energy. The total experimental resolution was ~ 180 meV and the spot size on the sample was $200 \times 30 \mu\text{m}$. The electronic band structure was measured with ARPES at the IFW-Dresden using a photoemission spectrometer equipped with a Scienta SES-200 hemispherical electron-energy analyzer and a high-flux He-resonance lamp (Gammadata VUV-5010). All ARPES spectra were acquired at a photon energy of $h\nu=40.8$ eV (He II α) with an angular resolution of 0.3° and a total-system energy resolution of 50 meV.

Acknowledgements

A.Grüneis acknowledges an APART fellowship from the Austrian Academy of Sciences and a Marie Curie Individual Fellowship ("COMTRANS") and travel support from the EU. D.V. acknowledges the Deutsche Forschungsgemeinschaft (Grant VY 64/1-1). We are grateful to A. Goldoni, S. Lizzit and P. Vilmercati for their support at the SuperESCA beamline and to R. Hübel for his support at the IFW-Dresden.

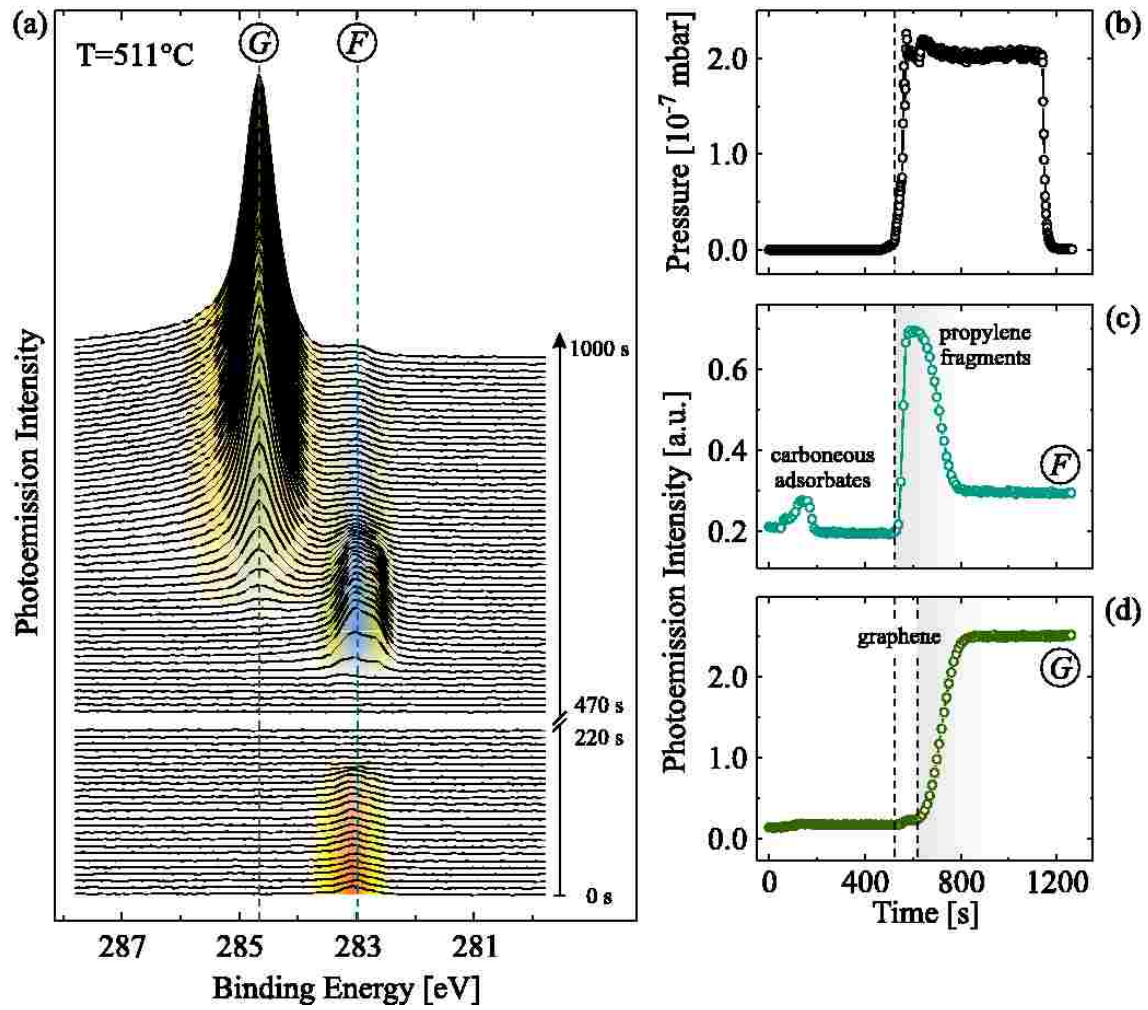


FIG. 1: (a) Time evolution of the PE intensity in the C 1s region during the graphene growth. F and G mark the signals from C_3H_6 fragments and graphene. (b) Partial C_3H_6 pressure. (c) and (d) Intensity of the fragment and the graphene C 1s PE signal integrated over ± 0.5 eV around their peak maximum.

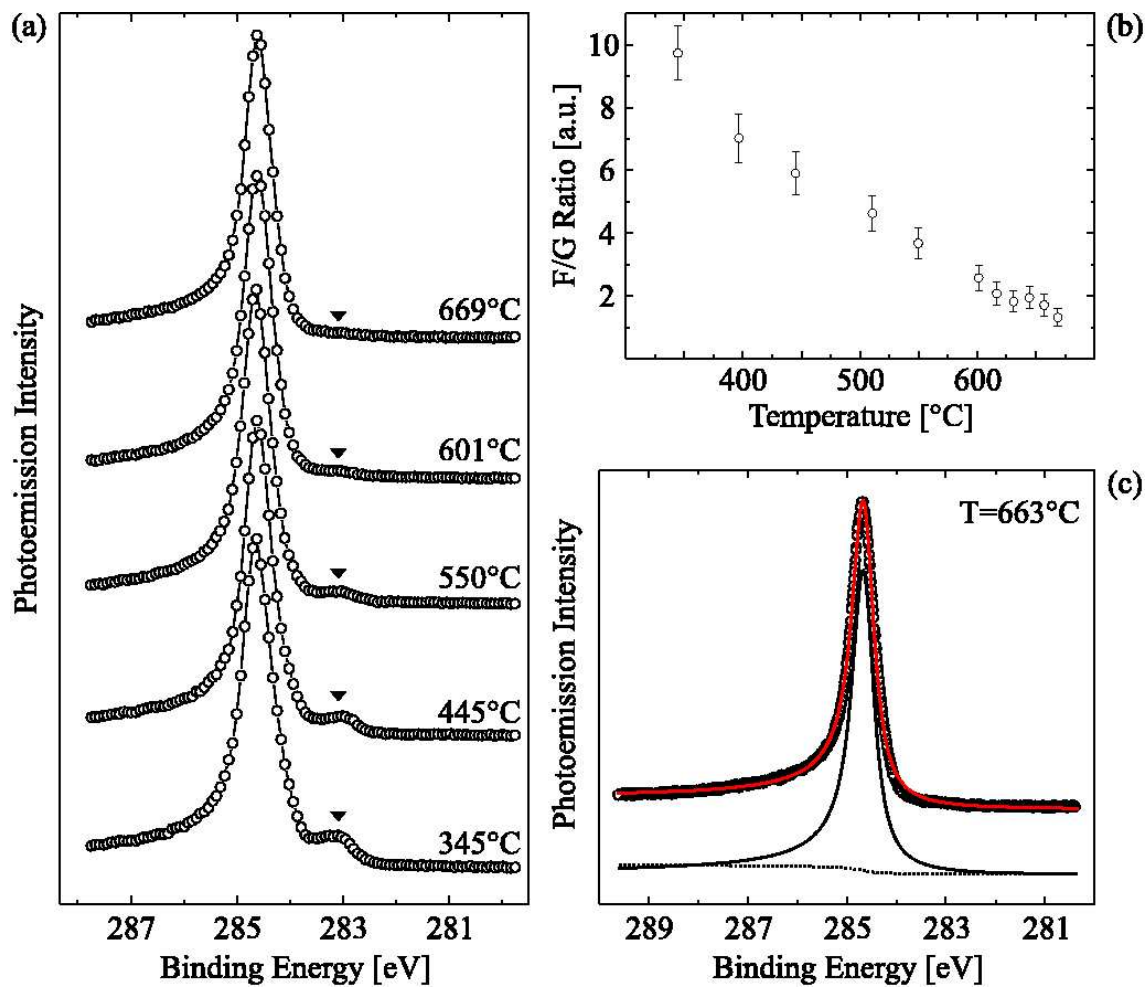


FIG. 2: (a) C 1s PE spectrum of the fully grown graphene layer for different temperatures. (b) Fragment to graphene PE intensity ratio as a function of synthesis temperature. (c) High resolution C 1s spectrum for graphene on Ni(111) along with a Doniach-Sunjc lineshape analysis (red line).

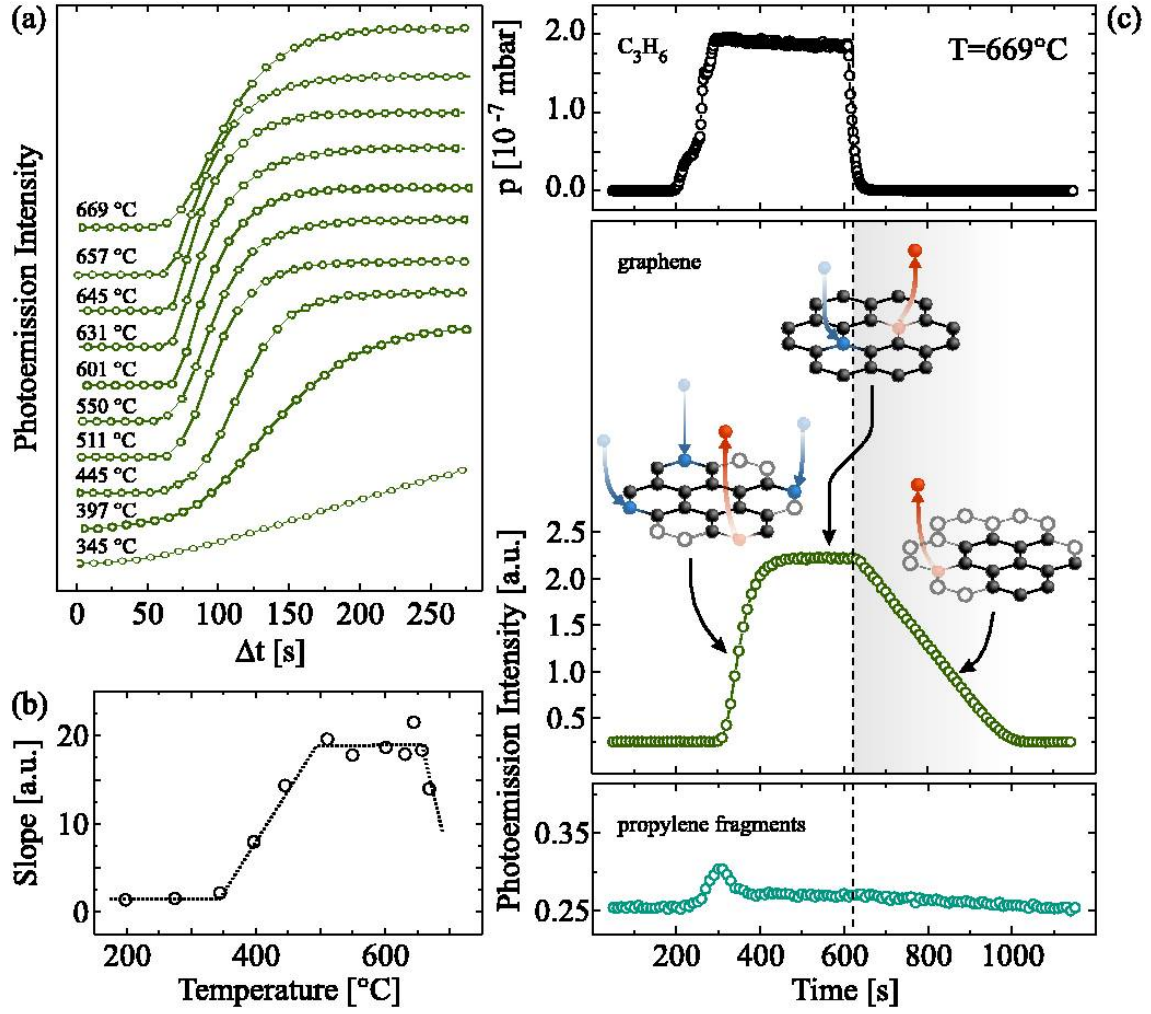


FIG. 3: (a) Time evolution of the graphene C 1s intensity for different temperatures. (b) Graphene growth rate as a function of synthesis temperature. (c) Graphene C 1s intensity spectrum for $T=669^\circ\text{C}$ indicating three consecutive development stages: rapid growth, a metastable phase, and desorption or diffusion.

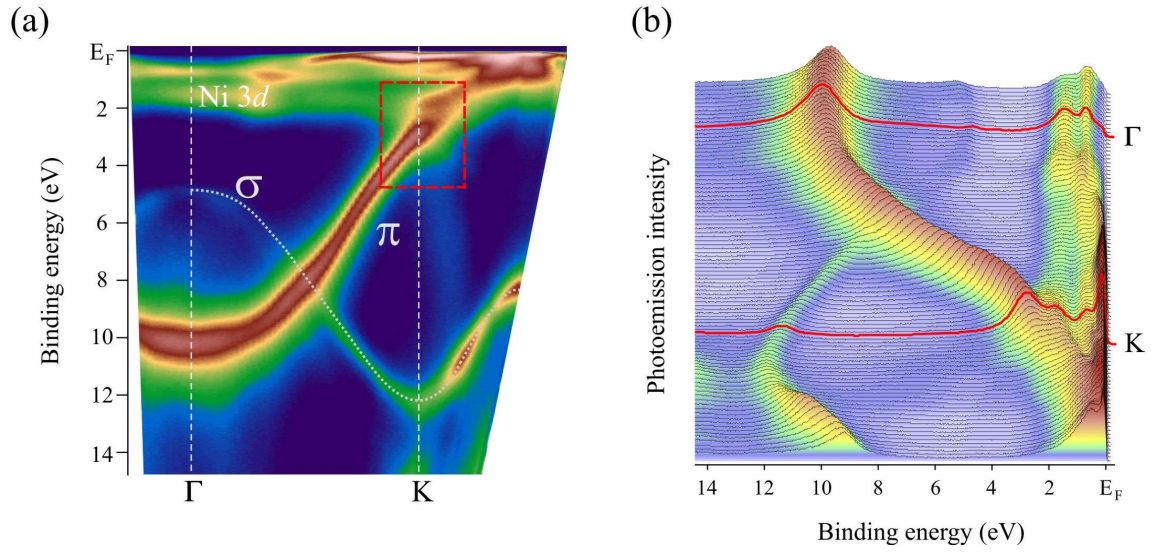


FIG. 4: (a) Band structure mapping by ARPES of a graphene monolayer synthesized at 550 °C. The graphene derived π and σ bands and the Ni 3d bands are depicted. The region around K denoted by a dashed rectangle exhibits the gap in the π band structure, which is due to substrate interaction. (b) The raw ARPES spectra: red lines denote scans taken at Γ and K points, respectively.

-
- [1] Novoselov, K. S.; Geim, A.K.; Morozov, S.V.; Jiang, D.; Zhang, Y.; Dubonos, S.V.; Grigorieva, I.V.; Firsov, A.A. *Science* **2004**, *306*, 666.
- [2] Geim, A.K.; Novoselov, K.S. *Nature Mat.* **2007**, *6*, 183.
- [3] Dedkov, Y.; Fonin, M.; Rüdiger, U.; Laubschat, C. *Appl. Phys. Lett.* **2008**, *93*, 022509.
- [4] Seyller, T.; Emtsev, K.; Gao, K.; Speck, F.; Ley, L.; Tadich, A.; Broekman, L.; Riley, J.; Leckey, R.; Rader, O.; Varykhalov, A.; Shikin, A. *Surf. Sci.* **2006**, *600*, 3906.
- [5] Xiaolin, L.; Guangyu, Z.; Xuedong, B.; Xiaoming, S.; Xinran, W.; Enge, W.; Dai, H. *Nature Nanotech.* **2008**, *3*, 538.
- [6] Niyogi, S.; Bekyarova, E.; Itkis, M. E.; McWilliams, J. L.; Hamon, M. A.; Haddon, R. C. *J. Am. Chem. Soc.* **2006**, *128*, 7720.
- [7] Gilje, S.; Han, S.; Wang, M.; Wang, K. L.; Kaner, R. B. *Nano Letters* **2007**, *7*, 3394.
- [8] Stankovich, S.; Dikin, D. A.; Dommett, G. H. B.; Kohlhaas, K. M.; Zimney, E. J.; Stach, E. A.; Piner, R. D.; Nguyen, S. T.; Ruoff, R. S. *Nature* **2006**, *442*, 282.
- [9] Schniepp, H.; Li, J.-L.; McAllister, M.; Sai, H.; Herrera-Alonso, M.; Adamson, D.; Prud'homme, R.K.; Car, R.; Saville, D.; Aksay, I. *J. Phys. Chem. B* **2006**, *110*, 8535.
- [10] Rader, H.; Rouhanipour, A.; Talarico, A.; Palermo, V.; Samori, O.; Mullen, K. *Nature Mat.* **2006**, *5*, 276.
- [11] Grüneis, A.; Vyalikh, D. *Phys. Rev. B* **2008**, *77*, 193401.
- [12] Nagashima, A.; Tejima, N.; Oshima, C. *Phys. Rev. B* **1994**, *50*, 17487.
- [13] Gamo, Y.; Nagashima, A.; Wakabayashi, M.; Oshima, C. *Surf. Sci.* **1997**, *374*, 61.
- [14] Karpan, V.M.; Giovannetti, G.; Khomyakov, P.A.; Talanana, M.; Starikov, A.A.; Zwierzycki, M.; van den Brink, J.; Brocks, G.; Kelly, P.J. *Phys. Rev. Lett.* **2007**, *99*, 176602.
- [15] Loginova, E.; Bartelt, N.C.; Feibelman, P.J.; McCarty, K.F. *New J. Phys.* **2008**, *10*, 093026.
- [16] Tanaka, K.; Hirano, H. *Catalysis Lett.* **1992**, *12*, 1.
- [17] Kovács, Gy.J.; Bertóti, I.; Radnóczy, G. *Thin Solid Films* **2008**, *516*, 7942.
- [18] Mongeot, F.; Toma, A.; Molle, A.; Lizzit, S.; Petaccia, L.; Baraldi, A. *Phys. Rev. Lett.* **2006**, *97*, 056103.
- [19] Nikitin, A.; Ogasawara, H.; Mann, D.; Denecke, R.; Zhang, Z.; Dai, H.; Cho, K.; Nilsson, A. *Phys. Rev. Lett.* **2005**, *95*, 225507.

- [20] Preobrajenski, A.B.; Ng, M.L., Vinogradov, A.S., Martensson, N. *Phys. Rev. B* **2008**, 78, 073401.
- [21] Siegel, D.J.; Hamilton, J.C. *Phys. Rev. B* **2003**, 68, 094105.
- [22] Lander, J.; Kern, H.; Beach, A. *J. Appl. Phys.* **1952**, 23, 1305.
- [23] Diamond, S.; Wert, C. *Trans. Metall. Soc. AIME* **1967**, 239, 705.
- [24] Kämper, K.-P.; Schmidt, W.; Güntherodt, G.; Kühlenbeck, H. *Phys. Rev. B* **1988**, 38, 9451.